University of Groningen

Topological Considerations on the Use of Batteries to Enhance the Reliability of HV-Grids

Fiorini, L.; Aiello, M.; Poli, D.; Pelacchi, P.

IMPORTANT NOTE: You are advised to consult the publisher's version (publisher's PDF) if you wish to cite from it. Please check the document version below.

Document Version
Final author's version (accepted by publisher, after peer review)

Publication date:
2018

Link to publication in University of Groningen/UMCG research database

Topological Considerations on the Use of Batteries to Enhance the Reliability of HV-Grids

L. Fiorini[a,*], M. Aiello[a,b], D. Poli[c], P. Pelacchi[c]

[a]*Department of Distributed Systems, University of Groningen, 9747 AG, Groningen, The Netherlands*
[b]*Department of Smart Energy Systems and Services, University of Stuttgart, Universitätsstraße 38, 70569, Stuttgart, Germany*
[c]*Department of Energy, Systems, Territory and Construction Engineering, University of Pisa, Largo Lucio Lazzarino, 56122, Pisa, Italy*

Abstract

The large amount of renewable energy sources (RESs) recently integrated within the electric power systems across the world poses new challenges for their operation. Among several viable solutions, energy storage systems are the most promising to increase reliability and flexibility. This paper proposes a novel topological and probabilistic approach to find the optimal capacity and siting of energy storage devices, in order to increase the system reliability and the hosting capacity of renewables. Wind and solar productions, generators availability, and real-time demand are modeled with proper distribution functions, and the yearly expected energy not supplied is estimated using a sequential Monte Carlo technique. Four siting policies are applied and compared to place the optimal storage capacity on eight grids with different topological characteristics. Power flows are linearized and the optimization of resources is formulated as a linear programming problem. The results show that large-scale batteries operated by the Transmission System Operator can significantly improve system reliability and exploitation of RESs. The presence of energy-hubs and small-world properties strongly increase the transmission effectiveness of weakly- and well-meshed grids. A siting policy based on the Power Transfer Distribution Factors matrix of the grid turns out to be particularly successful.

Keywords: Sizing, Siting, Reliability, Power Transfer Distribution Factors, Small-worldness, Preferential attachment

NOMENCLATURE

V, E	Set of all nodes and edges, respectively

---

*Corresponding author
   Email addresses:* `l.fiorini@rug.nl` (L. Fiorini), `m.aiello@rug.nl` (M. Aiello), `davide.poli@unipi.it` (D. Poli), `paolo.pelacchi@ing.unipi.it` (P. Pelacchi)

$T, \bar{T}$	Set of installed and on-line conventional generators, respectively
W, S	Set of wind and solar-PV farm, respectively
L, B, I	Set of loads, batteries, and bus bars, respectively
α	Modulation margin
c_{off1}, c_{off2}	Price of modulation power steps (€/MWh)
$cost_{CR}$	Cost of RES curtailment (€/MWh)
$cost_{EENS}$	Cost of EENS (€/MWh)
P^{max}, P^{min}	Rated power output and technical minimum power of a generator (MW)
RU, RD	Ramp Up/Down of conventional generators (MW/h)
Off_1, Off_2	Step limit for modulation power (MWh)
P_p	Produced power at forecasting stage (MW)
P_{av}	Available renewable power at forecasting stage (MW)
D_{ex}, D_{ex}^{st}	Expected demand at forecasting stage(MW)
D_s	Served power at forecasting stage (MW)
D_{real}, D_{real}^{st}	Real-time demand (MW)
st_t	Real-time state of conventional generator (1/0)
P_{MC}	Real-time available renewable production (MW)
P_{off}	Production for modulation purposes (2 steps) (MWh)
ch^{max}, SoC^{max}	Storage power and energy capacity (MW, MWh)
SoC^{min}	Minimum level of stored energy (MWh)
$StDis, StCh$	Power exchanged between storage and grid (MW)
η_{ch}, η_{dis}	Battery's efficiency in charging and discharging operations
r, LE	Interest rate and expected life of equipment (years)
c_{en}, c_{pow}	Battery investment costs (€/MWh, €/MW)

1. Introduction

In recent years, a large amount of renewable energy sources (RES) has been integrated within the electric grids across the world, in order to fulfill the goals of bold energy policies. For instance, the European Commission has set the targets to increase the energy efficiency by 20% and the share of renewables to 20% by 2020 [1]. The American Department of Energy prescribed that wind energy should contribute to 20% of electricity consumption by 2030 [2]. As a consequence, the uncontrollable and uncertain nature of RES poses new challenges to the operation of power systems, possibly affecting their reliability. Several viable solutions have been investigated in the recent scientific literature, such as demand management [3], the upgrade and expansion of the transmission grid [4], and energy storage systems. As network renovation and expansion may not be always technically feasible [5] and encounter strong public opposition [6], energy storage systems can defer large investment in high-voltage and distribution grid assets [7, 8], while increasing transmission capability [9]. Among several storage technologies, batteries and underground CAES are promising solutions for grid support and load shifting [5, 10, 11] so as to increase system reliability and flexibility, which is necessary to accommodate high shares of RES generation [12]. The use of batteries for load shifting purposes has been proved to be cost-effective for small renewable systems and medium-scale institutions in several US and European countries. For instance in Italy [13], a battery system would be economically advantageous for a public institution if a time-of-use tariff with significant difference between maximum and minimum electricity prices is applied, and it will be even more convenient in the near future thanks to the

already declining costs of energy storage devices. The reliability of the bulk power system, that is to say of the combination of generation, transmission, and HV nodal loads, is also affected by the grid topology, especially in terms of blackouts' frequency and magnitude [14, 15, 16].

In this work, a topological and probabilistic approach is proposed to find the optimal storage capacity to increase the system reliability and the use of renewables, addressing the first following research question: *What is the optimal size of storage systems in order to improve the reliability of bulk power systems, under production and demand uncertainties, and in a market environment?* In this paper, we take a graph-theoretical perspective, considering power systems modeled as weighted graphs [17]. The effects of constrained power flows and different topologies are evaluated before and after the allocation of large-scale batteries, assuming four siting policies. In this way, the second research question is addressed: *What are topologically-optimal locations to place the storage devices in order to improve the power system reliability?* To answer these questions, a modified version of the IEEE-RTS 96 with RES plants is used as reference grid and as the basis to generate other seven test networks with different topological characteristics. RES production, generators' availability, and real-time demand are modeled with probability density functions (PDFs) and estimated via a sequential Monte Carlo method (MC). A simplified three-stage model of the electricity market is adopted to assess the working point of the system during four representative days, which present typical Italian seasonal demand trends and varying weather conditions. Reduction in operation costs is compared with storage investment expenses to determine the optimal capacity. Then, the system reliability of different test cases is compared, and several storage systems are placed according to topology-driven siting policies. The results show that energy storage equal to 20% of the installed RES capacity can significantly reduce the amount of Expected Energy Not Served (EENS) and the excess of renewable production to curtail. The declining trend in storage costs allows to be optimistic about a future increase in applications [18, 19], as batteries are well suited to cope with the growing amount of installed RES and the consequent need for improving the transmission capacity and system flexibility [5].

From a topological point of view, small-world and preferential-attachment models exhibit the best performances, in terms of exploitation of RES and system reliability, among the cases with low and high average degree, respectively. The siting analysis evidences that installing one centralized storage device is usually the worst solution. Among the decentralized policies, effective results are achieved when batteries are located according to the Power Transfer Distribution Factors matrix (PTDF) of the grid.

The main contribution of this paper consists in proposing a novel approach based on the combination of a graph-theoretical perspective with a probabilistic reliability analysis, in order to investigate to what extent the network topology could provide insights in the optimal siting of energy storage systems.

The remainder of the paper is organized as follows. Section 2 provides an overview of the state of the art on the main ingredients of the study: storage

sizing and siting problem, on the one hand, and the influence of the topology of HV transmission grids on the bulk power system reliability, on the other hand. Section 3 briefly introduces the Monte Carlo method and the simplified market model used in this study. Section 4 provides the main features of the sizing and siting policies, together with some fundamental concepts for their definition. Section 5 and Section 6 explain the minimization problem to be solved and the details of the test cases, respectively. Results are presented in Section 7, followed by conclusions in Section 8.

2. State of the art

While the sizing and siting of batteries for transmission grids are becoming increasingly investigated, taking a graph-theoretical perspective in combination with a probabilistic approach is, to the best of our knowledge, a novel research line that could improve planning tools. We briefly overview the state of the art in these fields separately.

2.1. Sizing and siting of storage systems

Several methodologies are available in the literature to optimize the storage size in power systems with renewable sources, often associated with the investigation of its optimal operation. The studies in [20] and [21] propose methods for the scheduling and operation of generic storage devices in a market system. In both papers, the objective is to maximize the revenue for renewable power plants owners. In the first work, the owner can take advantage of variations in the spot price by shifting energy over time, whereas in the second work, wind plants participate in ancillary service markets. In [21], a deterministic framework is considered, whereas in [20] wind farm output is probabilistically determined and the storage is operated in order to smooth unexpected variations. A deterministic framework is also considered by the authors of [22], who adopt a vertically-integrated approach. The optimal capacity results from the minimization of traditional generation and storage investment cost. A similar approach is found in [23], whose authors use probability density functions (PDFs) to model the stochastic nature of wind speed and load. Total costs of generation and load shedding are minimized to seek the optimal capacity of CAES, whose investment costs are compared to conventional gas-fired alternatives. The main objectives of this study and of [24] are the enhancement of system reliability and wind integration. In the latter, the stochastic behavior of wind speed is simulated with the ARMA time-series model. Expected Energy Not Supplied (EENS) and the Expected renewable Energy Not Used (EENU) offer an index of system reliability improvement by adding batteries. In [25], Markovian functions are assumed to govern renewable generation, demand, and electricity prices; the main goal is to minimize the long-term average cost of conventional generators, as well as investment in storage, while satisfying all the demand. The authors of [26] propose a probabilistic method for determining the optimal size of on-site storage and transmission upgrades needed to connect

4

wind generators to power systems, while improving their reliability and the use of available transmission capacity. In [27], the authors discuss the financial viability of installing bulk batteries to reduce the curtailment of wind energy and improve the performance of the power grid in northern Vermont. With a similar aim, both ESS and transmission expansion are jointly investigated as possible technologies in [8], where the proposed MILP problem is applied to two test systems, and in [12], where a cost/benefit analysis is conducted for Central Western Europe and Nord Pool grids. In [28], we perform an investigation of how proper sizing (and, to a smaller extent, siting) of large-scale batteries can enable a smarter use of the transmission grid with a high share of renewable, assuming a deterministic framework. Optimal sizing and siting problems are jointly investigated with a three-stage approach in [29]. Starting from an idealized situation where storage is available in any capacity at any node, the optimal size is determined averaging over one year the daily maxima of stored energy and exchanged power. Only locations with the highest contribution in lessening transmission congestions are identified as valuable ones. Time series models of wind speed data are used to obtain the deterministic wind forecast. Storage allocation is the first main goal of [30], together with the storage portfolio optimization. The optimal siting problem is addressed by minimizing production costs, storage operation, and maintenance costs. Wind production is considered as known data as well as the demand, and several technologies are considered. A greedy algorithm is used in the aforementioned [22] to choose the nodes where to place storage devices, starting from storage available at all nodes, and shrinking their numbers while improving performances at each iteration. Genetic algorithm-based approaches for storage allocation are proposed in [23, 31, 32]. In [31], a market-based optimal power flow assuming generator marginal costs as an input determines the unit (de)commitment for each hour and local marginal prices to minimize the hourly social costs. The study concludes that co-locating storage and wind farms enhances the performance of wind integration. However, different conclusions are drawn in [23, 22, 30, 28], where the storage is found to be optimally located in buses other than close to renewable generators, mainly due to network congestions.

In this paper, we propose a probabilistic and topological approach to address the storage sizing and siting problem, by taking the TSO's point of view to improve system reliability and increase the hosting capacity of renewable sources. To the best of our knowledge, little work has been done on this topic. The sizing problem is addressed by minimizing the operation costs due to EENS and curtailment of renewable energy in excess. Stochastic nature of RES generation, load, and generators' availability are modeled with PDFs and a Monte Carlo method is used to compare the benefits of storage with respect to its investment costs. A simplified model of the electricity market is considered for the day-ahead and real-time operation of conventional generators; batteries are used by the TSO only as a last resort to balance the grid. Then, the allocation of batteries in eight different grids is investigated by means of four siting policies related to topological network characteristics.

5

2.2. Network topology and bulk power system reliability

Chassin and Posse propose a method to estimate the loss-of-load probability reliability index of a power system based on the Barabási-Albert scale-free network model [33]. Holmgren models power networks as graphs and evaluates the effects of random failure and deliberated attacks to high degree nodes in terms of unserved energy [34]. Two real power grids, a scale-free network, and a random graph are used as test cases. The latter appears to be the less vulnerable to external attacks than the other cases, and, in general, all networks are more vulnerable to deliberated attacks than challenged by random failures. The unserved energy index is used in [35] to compare the effects of strategic attacks when removing critical components identified by conventional betweenness or by an electrical one. The results show that the proposed metric gives a better indication of the grid weakness. Roughly ten years of blackouts within European transmission grids are investigated in [14] and [15]. Reliability indexes conceived for power systems (energy not served, loss of power, and restoration time) are correlated with transmission grid topologies. Both studies conclude that more interconnected systems are more frequently subject to fault events, but these have a smaller impact than in grids presenting less meshed and more randomly-generated topologies. Exposure to cascading failure in power grids with high connectivity and clustering is investigated in [36]. Long-edges connecting nodes far from each other are found to be the weakest elements of the grid, as their failure causes the reroute of a significant amount of energy, leading to cascading effects. It is suggested that a more reasonable configuration of the grid would be more effective than increasing its capacity. We provide a comprehensive survey on topological and network models of electricity transmission and distribution grids in [37], while we propose novel topological metrics in [38] and techniques to identify grid weaknesses in [39].

Previous network theoretical studies consider simple models of power systems [37]. The vast majority neglects physical properties of the lines, but focuses mainly on simple connectivity relations. Furthermore, most studies investigate the system robustness to outages or external attacks by removing nodes and edges, and not in terms of system adequacy and security, in particular concerning the optimal placement and operation of batteries.

In the present study, we investigate to what extent different grid topologies may affect the optimal siting of storage devices devoted to reducing EENS and maximizing the production of RES, while coping with a secure operation of the bulk power system, i.e., of transmission and generation assets. In this paper, the concept of reliability refers to both adequacy (are generation, transmission, and storage assets well sized and sited?) and system security (is the use of resources well scheduled and operated, in order to face real-time contingencies and unavoidable power unbalances?). Both aspects are in fact captured by reliability indexes such as EENS, whose value depends on availability, dispatching, and on-line operation of resources.

6

3. Approach and Operation Phases

Our approach to coping with the variability of generation, storage and demand, is probabilistic. It is based on the Monte Carlo method, that is a stochastic simulation using (pseudo-) random numbers [40, 41, 42, 43]. We employ different PDFs to estimate the availability of each conventional generator, the renewable production, and the expected load error. If a generation unit fails at a given time step, it is unavailable also during the following ones, until the failure is repaired; the real-time load demand is determined by considering the cumulative error. As each system state is dependent on the previous ones, the applied method is often called *sequential*. Further details of our use of the Monte Carlo method are presented in Appendix A.

As for the market environment, we adopt a simplified model to assess the scheduled working point of each generation unit during the simulated days. The system operation is reduced to three main steps (forecast, normal, and contingency operation) and an hourly discretization is considered for the whole simulation. The *forecast operation* defines which units are committed to producing and at what level of power, for each hour of the following day. At this stage, load profiles are assumed to be deterministically known, their trends and peak-values are derived from the Italian TSO database [44, 28]. The wind speed is set equal to the seasonal average for the whole day, whereas the solar production is estimated assuming clear sky conditions. All conventional generators are available and progressively dispatched to cover the load, according to an economic merit order list based on their marginal costs [45]. At the beginning of the real-time simulation of a day, an MC drawing is performed to calculate the hourly load forecasting error, the wind speed, the sky clearness index, and the actual availability of generators. If the expected production based on RES and conventional generators is still feasible and the system is balanced, the real-time hourly operation is simulated as scheduled (*normal operation*). If one or more outages or a significant error in load or RES forecasting are drawn by the Monte Carlo procedure, the substantial system unbalance requires the quick activation of the so-called *contingency procedure*. The significant gap between real-time load and available power must be covered by the modulation power of spinning units, according to a merit order list based on their two level of offers. Fast generators can also be turned off or on for the following hours, as replacement reserve. When these actions are not enough to meet the entire load, the TSO can provide balancing power by means of its storage devices, if available, by injecting into the grid energy previously stored or by charging them. As a last resort, the extra demand or renewable energy are subject to load shedding or curtailment, respectively. Although economic studies show that batteries become more cost-effective when used for multiple applications [46], how to integrate storage facilities within the regulatory environment is still an open problem [47]. In this work, we assume that the TSO uses its storage only after all power producers have procured and, potentially, been compensated for balancing services. Four days are simulated in order to represent different seasonal supply-demand scenarios by varying load profiles and expected renewable

productions [28].

4. Sizing and Siting

The aim of this study is to estimate the best size and location of large-scale batteries in transmission systems of various topological shapes, in order to increase the system reliability and to reduce the yearly Expected Energy Not Supplied (EENS). Consequently, this work is articulated in two parts: first, the best total size of storage is assessed by comparing the reduction of the annual operation cost obtained assuming a single busbar model, with the costs of investment and O&M of storage; second, the best location is found by comparing the effects of four siting policies on grids with different topological structure. In the following sections, we present methodologies for sizing and siting of storage, as well as some background on both power systems and complex network analysis.

4.1. Sizing

The total size of storage to add to the grid is determined by means of an economic evaluation of the annualized costs for installing, operating, and maintaining batteries and of the potential benefit of the storage in terms of reduction of the annual operation costs (OC); these include the cost of load shedding and a penalty for curtailing renewable energy.

Several configurations are simulated with the same generation park, while storage systems are added to the grid as one centralized large-scale battery, whose power capacity varies from 10% to 100% of the installed renewable capacity, in 8 steps. The storage system is used for the energy-intensive application of energy shifting over time. According to EPRI's studies [5, 48], batteries are one of the most flexible and attractive technologies for grid support and load shifting. Among the available types, the Sodium-Sulfur (NaS) technology is already applied in several areas (Japan, USA, Europe, UAE) and considered one of most promising solution for this application [49]. Therefore, its typical energy to power ratio and charge/discharge efficiency are adopted, i.e, 6 hours and 87%, respectively. Moreover, an all-inclusive cost of 500 k€/MWh is considered and annual O&M costs are assumed to be 3% of the investment [48], [50].

4.2. Siting

The second part of this work consists of comparing in terms of system reliability the effects of four siting policies on similar grids that differ only for their topological characterization. Transmission grids are topologically represented as a graph, with nodes and edges [51, 17, 37]. The first ones are distinguished in sinks, sources, and inner nodes, corresponding to generators, loads, and busbars, respectively. The second ones represent the transmission lines and are characterized by a weight, i.e., the reactance, and three levels of power capacity: continuous rating (CR), long term-emergency rating (LTR), and emergency rating (ER). The first two limits are set according to the IEEE-RTS 96 [52], while the latter is 10% higher than LTR.

8

4.2.1. PTDF

The Power Transfer Distribution Factors matrix (PTDFs) expresses the influence of each nodal power injection on every line. In this work, a DC-PTDF is considered; it is based on the linearized DC power flow and mainly affected by the grid topology [53, 54]. The DC power flow is a useful approximation of AC power flow and is frequently adopted at the transmission level, when voltage stability is not investigated (e.g. [53, 30, 22]). The DC-PTDF matrix can be used to evaluate the change in power flow on lines due to nodal injections, hence, given the PTDF of a network, one can try to change the power flow on an edge by supplying or withdrawing power from a node. For further details, we refer to [53].

4.2.2. Utilization index and Flow-based nodal centrality

In [28] we define the *Utilization index* to assess the usage of the edge capacity. Let P_e be the power flow passing through the edge e and let CR_e be its continuous rating capacity; the *Utilization index* $U(e)$ is then defined as:

$$U(e) = P_e/CR_e \tag{1}$$

If $U(e) \leq 1$, the edge is in a normal state, while if $U(e) > 1$ the edge is overloaded or in an emergency state. Adjusting the power flows in real-time to relief overloaded lines is out of scope of this work, nevertheless the Utilization index is useful to identify and rank the most stressed lines. The *Flow-based nodal centrality* is used to identify the nodes that dispatch a higher amount of power among the grid, having a more central role within the network than those less active. According to [55], if P_{ij} is the positive power flow from node i to node j during a single time step; P_{tot} is the total power flowing on the grid in the same time step; $\Gamma(i)$ is the set of adjacent nodes to i, i.e., a real edge connects them; then, the Flow-based nodal centrality index of node i, $C_f(i)$, is defined as follows:

$$C_f(i) = (\sum_{j \in \Gamma(i)} P_{ij})/(P_{tot}) \tag{2}$$

4.2.3. Siting Policies

Given the topology of a grid without storage, the real-time demand and production levels obtained from the simulation of its operation (see Section 3), we run simulations of the DC-load flows and consequently apply the just defined metrics. Then, four different siting policies are applied to add one or more storage systems: (a) placing them on the ten nodes with the highest average $C_f(i)$; (b) placing them close to the ten consumers most subject to load shedding; (c) placing them on the ten nodes connected to the ten most congested lines, ranked according to the PTDFs; and (d) placing them on the single node with the highest average $C_f(i)$.

According to their definitions, both $U(e)$ and $C_f(i)$ vary at each time-step; however, it is not possible to relocate batteries every 15 minutes. To use these metrics for locating the batteries, we need constant values. As regards policies

9

(a) and (d), the most active nodes are identified according to their average $C_f(i)$ over all simulations. With respect to policy (c), to identify the most stressed lines, for each edge e we count the time-steps during which it is overloaded or in emergency state, i.e., $U(e) > 1$, and we rank all real lines accordingly. Moreover, it is worth explaining that the element on row n and column l of the DC-PTDF matrix of a grid specifies which share of power flows on line l when one unit of power is injected at node n and extracted at a sink node. We set the sink node to be the slack bus used for running the OPF [56]. For each one of the top-ten congested lines l, we use the DC-PTDF to place a storage at the node n which corresponds to the smallest negative element PTDF(n,l), as we aim to lower the power flow on line l.

Choosing a different number of storage devices according to the test-case could have been an alternative approach. However, since this study investigates to what extent different topological characteristics can influence the optimal siting of batteries, we use in all cases the same amount of batteries in order to compare the effects of the siting policies on grids with different topologies but the same number of generators, loads, and storage nodes.

The resulting EENS, curtailed RES energy, number of hours with no feasible solution, and line congestions are considered as optimality functions to compare topologies and policies.

4.3. Topological measures

We distinguish edges as *real* and *virtual*. The *real* edges represent physical transmission lines between inner nodes, creating the main structure of grid, hereinafter referred to as the *core* of the network. Sinks and sources are considered external nodes and are linked to the core by *virtual* edges with a conventional weight of 10^{-4}, in order to characterize every node in a unique way. The grids used as test-cases (see Section 6) are described using topological measures derived from the complex network analysis field.

The *clustering coefficient* is a measure of the extent to which the adjacent nodes of node i are also adjacent to each other [57]. Therefore, it indicates the tendency of nodes to clustering together and it is defined by Watts and Strogatz as follows:

$$c_i = 2E_i/k_i(k_i - 1) \tag{3}$$

where E_i is the number of edges between the adjacent vertexes of i and k_i is the *degree* of node i, i.e., the number of edges incident to the node. The clustering coefficient of the grid, C, is the average of c_i over all vertexes.

The shortest path between two vertexes is the path among all possible ones with the least number of edges. Consequently, the *characteristic path length CL* of a network is the median of the shortest path lengths connecting each vertex to all other vertexes. According to Watts and Strogatz, a network is said "small-world" if the relations $C \gg C_{rand}$ and $CL \gtrsim CL_{rand}$ hold, where C_{rand} and CL_{rand} are the clustering coefficient and characteristic path length of a random graph having the same number of vertexes N and the same average degree $\langle k \rangle$. The authors of [58] proved that this is a categorical definition that does not allow

to measure to what extent a network has small-world properties. To address this problem, they propose a quantitative measure of "*small-worldness*:"

$$\sigma = (C/C_{rand}) \cdot (CL_{rand}/CL) \tag{4}$$

If $\sigma > 1$, then the network is said to be a small-world one.

5. Formulation

To formulate and solve the problem, we consider four phases: forecasting, contingency, sizing, and siting.

5.1. Forecasting Phase

The forecasting phase is used to determine for each time step which units are called to produce and at what level of power. The objective function to be minimized at every time-step h represents the total costs of production, curtailment, and expected energy not supplied (EENS):

$$
\begin{aligned}
min\Bigg\{ &\sum_{t \in T} c_t \cdot P_{p,t,h} + \sum_{s \in S} c_s \cdot P_{p,s,h} + \sum_{w \in W} c_w \cdot P_{p,w,h} + \\
&cost_{CR} \cdot \Bigg[\sum_{s \in S}(P_{av,s,h} - P_{p,s,h}) + \sum_{w \in W}(P_{av,w,h} - P_{p,w,h}) \Bigg] \\
&+ cost_{EENS} \cdot (D^{st}_{ex,h} - D_{s,h}) \Bigg\}
\end{aligned}
\tag{5}
$$

where the first three terms are the production costs, at their marginal costs c; the second term is the cost of RES curtailment; last term is the cost of EENS. The value of renewable curtailment is set equal to 200 €/MWh, considering the actual Italian legislation on the compensation for RES reduction [59], while a realistic value of loss of load for firms, governments, and households is 8000 €/MWh, irrespective of the timing of the event [60].

The objective function is subject to several additional linear constraints:

$$P_t^{min} + \alpha \cdot P_t^{max} \le P_{p,t,h} \le P_t^{max} \cdot (1 - \alpha) \tag{6}$$

$$P_{p,t,h-1} - RD_t \le P_{p,t,h} \le P_{p,t,h-1} + RU_t \tag{7}$$

$$0 \le P_{p,r,h} \le P_{av,r,h} \le P_{p,r}^{max} \tag{8}$$

$$\sum_{t \in T} P_{p,t,h} + \sum_{s \in S} P_{p,s,h} + \sum_{w \in W} P_{p,w,h} = D_{s,h} \tag{9}$$

where Equation (6) guarantees $\forall t \in T$ that conventional plants can participate to real-time balancing, given a modulation margin $\alpha = 7\%$. Equation (8) limits renewable productions $\forall r \in S \cup W$. Equation (7) takes into account upper

and lower ramp generation limits $\forall t \in T$, while Equation (9) guarantees the supply-demand balance, considering a single busbar model.

As during night hours the electricity price is usually low, it is assumed that from 10 p.m until 4 a.m. the batteries' owner (TSO) buys an amount of energy corresponding to 25% of their capacity or until they are fully charged. Therefore, the total expected load to supply at this stage $D_{ex,h}^{st}$ is higher than the consumers' expected demand $D_{ex,h}$.

5.2. Contingency Procedure

Once the actual real-time consumers' demand $D_{real,h}$ and available production are determined by using the MC technique, the unbalance is calculated as follows:

$$\Delta P_h = D_{real,h}^{st} - \sum_{t \in T} st_{t,h} \cdot P_{p,t,h} - \sum_{s \in S} P_{MC,s,h} - \sum_{w \in W} P_{MC,w,h} \qquad (10)$$

If $\Delta P_h = 0$, the hourly operation is simulated as planned; otherwise, the contingency procedure is activated. Two scenarios can be distinguished depending on whether ΔP_h is positive or negative. The general objective function is:

$$min\left\{\sum_{t \in \bar{T}} (P_{off1,t,h} \cdot c_{off1,t} + P_{off2,t,h} \cdot c_{off2,t}) + cost_X \cdot X_{c,h}\right\} \qquad (11)$$

where the subscripts *off1* and *off2* refer to the first and second steps of offers necessary to increase (if $\Delta P_h > 0$) or decrease (if $\Delta P_h < 0$) production. Analogously, X_c is the EENS or the curtailment. Equation (11) is subject to the following linear constraints:

$$0 \leq P_{off1/2,t,h} \leq Off_{1/2,t} \qquad (12)$$

$$0 \leq EENS_{c,h} \leq D_{real,h}^{st} \qquad (13)$$

$$0 \leq curt_{c,h} \leq \sum_{s \in S} P_{MC,s,h} + \sum_{w \in W} P_{MC,w,h} \qquad (14)$$

$$\sum_{t \in \bar{T}} (P_{p,t,h} \pm P_{off1,t,h} \pm P_{off2,t,h}) + \sum_{s \in S} P_{MC,s,h} + \sum_{w \in W} P_{MC,w,h} = D_{real,h}^{st} \mp X_{c,h}$$
$$(15)$$

Equation (12) sets the limits on first and second steps of modulation power $\forall t \in T$; Equation (13) and Equation (14) refer to the maximum possible EENS and curtailment, respectively; Equation (15) guarantees the demand-supply balance, considering a single busbar model.

If there is still an unbalance, fast generators are turned off or on for the current time-step and the same algorithm is run again. As a last resort, the TSO uses the storage to reduce the final curtailment of RES or load.

At the end of each time step h, the battery's state of charge at the beginning of next time-step SoC_{h+1} is updated: if the storage discharges, $StDis_h > 0$, then Equation (16) applies, whereas if it charges, $StCh_h < 0$, Equation (17) is used.

$$SoC_{h+1} = SoC_h - StDis_h/\eta_{dis} \tag{16}$$

$$SoC_{h+1} = SoC_h + StCh_h \cdot \eta_{ch} \tag{17}$$

As apparent, the model conceived for the energy storage is very general and not constrained or limited to a specific technology (pumped-storage power plants, batteries, CAES, etc).

5.3. Economic Evaluation for Sizing

Simulations based on the MC technique halt upon the fulfillment of a stopping criterion or a prefixed limit of iterations, set to twenty thousand. The stopping criterion is that the relative standard deviation (RSD) of the EENS decreases below 5% [61, 62].

The expected annual energy not supplied $EENS_{year}$ in MWh is derived from the average EENS obtained over all 4-days simulations by applying a factor of 91.25. The expected annual curtailment $Curt_{year}$ is calculated accordingly.

Then, the annual OC, the annualized IC and O&M costs of storage are calculated respectively as follows:

$$OC_{year} = EENS_{year} \cdot cost_{ENS} + Curt_{year} \cdot cost_{CR} \tag{18}$$

$$IC_{year} = \frac{r(1+r)^{LE}}{(1+r)^{LE} - 1} \cdot (c_{en} \cdot SoC^{max} + c_{pow} \cdot ch^{max}) \tag{19}$$

$$O\&M_{year} = 0.03 \cdot IC_{year} \tag{20}$$

where $r = 5\%$ and LE=13 years. The case without any batteries is used as the baseline. Since this work investigates the potential benefits deriving from the installation and operation of storage devices in HV-grids, these are considered cost-effective if they enable a reduction of OC that is higher than their equivalent annual costs EAC, where $EAC = IC_{year} + O\&M_{year}$. The EAC is the cost per year of owning, operating, and maintaining an asset over its entire expected life. It is often used to assess if a project is financially viable [63]. The optimal total size of the storage devices to be installed is evaluated according to the procedure described in Section 4.1. An alternative approach could be the maximization of the gap between EAC and OC, but it would shift the focus to more economic aspects, and it would limit the potential improvements in terms of system reliability and use of renewables. Hence, further financial analysis, e.g., detailed business plans and speculative use of storage devices by the TSO are out of the scope of this paper.

5.4. DC load flow for Siting

Given the outputs coming from the sizing procedures and focusing on the grid structure under investigation, a DC optimal power flow (OPF) is run to mini-

13

mize the real-time OC. The flow on a line between nodes i and j during hour h, $P(i, j)_h$, is defined as:

$$P(i, j)_h = PB \cdot (\theta_i - \theta_j)/(x_{i,j}) \tag{21}$$

where θ_i, $x_{i,j}$, and PB are the voltage phase angle at node i, the reactance of the edge ij, and a base power of 100 MW, respectively.

The objective function is formulated as follows:

$$min\left\{ cost_{CR} \cdot \left[\sum_{s \in S} (P_{MC,s,h} - P_{f,s,h}) + \sum_{w \in W} (P_{MC,w,h} - P_{f,w,h}) \right] + \right. \\ \left. + cost_{EENS} \cdot \left[\sum_{l \in L} (D_{real,l,h} - D_{l,h}) \right] \right\} \tag{22}$$

where $P_{f,t,h}$ and $P_{f,r,h}$ are the conventional and renewable productions resulting from the sizing procedure, and $D_{real,l,h}$ are the nodal load values obtained from $D_{real,h}$ by using the percentages proposed in [52].

The objective function in Equation (22) is subject to the following linear constraints:

$$P(t, j)_h = P_{f,t,h} \quad \forall t \in T \tag{23}$$

$$0 \le P_{f,r,h} = P(r, j)_h \le P_{MC,r,h} \quad \forall r \in S \cup W \tag{24}$$

$$0 \le D_{l,h} = P(i, l)_h \le D_{real,l,h} \quad \forall l \in L \tag{25}$$

$$-c(i, j) \le P(i, j)_h \le c(i, j) \quad \forall (i, j) \in E \tag{26}$$

$$\sum_{(i,n) \in E} P(i, n)_h = \sum_{(n,j) \in E} P(n, j)_h \tag{27}$$

$$max\left\{ (-ch^{max})/(\eta_{ch}); -(SoC_b^{max} - SoC_{b,h})/(\eta_{ch}) \right\} \le P(b, i)_h \le \\ min\left\{ ch^{max} \cdot \eta_{dis}; (SoC_{b,h} - SoC_b^{min}) \cdot \eta_{dis} \right\} \quad \forall b \in B \tag{28}$$

$$\sum_{t \in T} P_{f,t,h} + \sum_{r \in S \cup W} P_{f,r,h} + \sum_{b \in B} P(b, j)_h = \sum_{l \in L} D_{l,h} \tag{29}$$

$$-\pi/2 \le \theta_{i,h} \le \pi/2 \quad \forall i \in V \setminus s \tag{30}$$

$$\theta_{s,h} = 0 \tag{31}$$

Constraints (23), (24), and (25) tie the power supplied from or to external nodes to the flow on the connected virtual edge. Renewable energy injected into the grid is bounded by the available one (Equation (24)), and loads cannot be provided with more power than requested (Equation (25)). Equation (26) limits power flowing on lines to their capacity. First, $c(i, j)$ is set equal to $CR(i, j)$

14

for all real edges; if there is no feasible solution, then the power flow for the current hour is run again with $c(i,j) = LTR(i,j)$. As a last resort, the capacity limit is set equal to ER; if the simulation does not succeed, i.e., no solution is found that satisfies all linear constraints and bounds, the program records a failure and goes to the next time-step. When a line is operated above its CR limit, it is considered in overloading but still in a secure state, whereas it is in emergency if above its LTR. Equation (27) guarantees the flow conservation at inner nodes, while Equation (28) determines the power flowing from or to batteries. Equation (29) guarantees supply-demand balance. Transmission losses are neglected. Equations (30) and (31) refer to phase angle constraints, where s is the slack node, and are required to solve the DC OPF problem.

6. Test Cases

Eight grids with different topologies are used as test-cases. A modernized IEEE RTS-96 bus, including Open Cycle Gas Turbines, Combined Cycle Gas Turbines, and Integrated Gasification Combined-Cycle generators, is used as reference network to build the others [52, 64]. This bus has an installed conventional generation capacity of 10.2 GW, to which we added 5.9 GW of RES plants, of which 5.25 GW are 250-MW large-scale wind farms, while the remaining power comes from PV-panels. The grid has a total transmission capacity of around 55.9 GW in CR and of 63.7 GW in LTR. From a topological point of view, the modified IEEE-RTS 96 has order 209 (that is the total number of nodes; 88 are inner nodes) and size 244 (that is the total number of edges; 123 are real edges), see Figure 1a. The average node degree $\langle k \rangle$ and clustering coefficient C of the core are 2.80 and 0, respectively. In particular, $C = 0$ means that the graph shows no clusters, i.e., it is a triangle-free graph.

Starting from the modified IEEE-RTS 96, seven grids are generated to investigate to what extent the topological structure can affect the system reliability in terms of EENS and use of RES energy. They have the same order and total transmission capacity, while the number of edges and the average node degree vary to allow for different shapes. As the reference bus has $\langle k \rangle = 2.8$, comparing grids with such an average degree is the fair choice; hence, we generate one random graph with $\langle k \rangle \approx 2.8$. Preferential-attachment and small-world networks require a fair amount of manual work to be generated with similar characteristics. We opt for networks with core average degree of 2 and 4. The clustering coefficient and small-worldenss values are calculated *a posteriori* till the right shape of the network is identified. The CR and LTR values for line power capacity are calculated as the average ones of the IEEE-RTS 96, given the test case size. Real edge weights are assigned by following the sequence of line reactances in the IEEE-RTS 96. Table 2 summarizes the main characteristics of test cases core.

Three random graphs are built according to one of the two model proposed by Erdős and Rényi in [65] to create the core of the grid. Two parameters are needed, i.e., order and size. If the resulting graph is disconnected, that means there is at least one pair of nodes such that no path has those nodes as endpoints,

Table 2: TEST CASES OVERVIEW

ID	Size	$\langle k \rangle$	C	S-W	Av.CR	Av.LTR
IEEE	123	2.8	0	✗		
RG	127	≈ 2.8	0.066	✗	417	501
RG4	176	4	0.037	✗	301	362
PA4	173	≈ 4	0.219	✓6.64	306	368
SW4	176	4	0.150	✓3.86	301	362
RG2	102	≈ 2.3	0.023	✗	519	624
PA2	87	≈ 2	0	✗	608	732
SW2	88	2	0	✗	601	723

For each test case, the following parameters are reported: size, average node degree, clustering coefficient, and small-world properties (yes ✓or no ✗) of the core; average continuous rating and long-term emergency rating of real edges.

one or more edges are added to get a connected core. The order is set equal to 88, while the size of the core is chosen to have $\langle k \rangle \approx 2.8$, $\langle k \rangle \approx 2$, and $\langle k \rangle = 4$. These graphs are referred to as RG, RG2, and RG4, (see Figure 1b).

The preferential attachment model of Barabási-Albert [66] is based on the idea that whenever a new node is added to the grid and linked to m other nodes, those with a higher degree are preferred for connection. We create two graphs whose cores have a preferential attachment structure; the order of the core is in both cases 88, while m is once 1 and once 2, resulting in $\langle k \rangle \approx 2$ and $\langle k \rangle \approx 4$. The final graphs are identified as PA2 and PA4; the former is shown in Figure 1c.

The small-world grids are built according to the model proposed by Watts and Strogatz [57], based on a "random rewiring procedure." Starting from a regular lattice, each edge is rewired with a random probability $p \in [0, 1]$. Thus, the resulting graph can be regular ($p = 0$), random ($p = 1$), or show intermediate properties. Three parameters are needed, i.e., order, p, and $\langle k \rangle$. The first two parameters are set for both networks equal to 88 and 0.4, respectively, while $\langle k \rangle$ can be equal to 2 or 4; the corresponding graphs are referred to as SW2 and SW4. The latter is represented in Figure 1d.

7. Results

The model and the objective functions presented in Section 5 have been implemented in MATLAB. Taking grid descriptions, expected load demand, and renewable production as input, we follow the described four phases of power flow simulation. Both the sizing and siting parts are linear programming problems; in the former, the "linprog" solver is used, while in the latter, due to the higher complexity of the constraints, the "GNU GLPK" library is preferred, by means of the GLPKMEX interface [67]. Graphs have been built and analyzed with the MATLAB Tools for Network Analysis available online, in particular, we use [68]. The Monte Carlo simulations have been run on one node Intel Xeon, 2.5 GHz of the Peregrine cluster of the University of Groningen [69]; for the DC-load flow simulations, the configuration of the computer hardware was: CPU Intel Core

(a) Modified IEEE-RTS 96

(b) RG with core size 127.

(c) PA graph with $\langle k \rangle \approx 2$

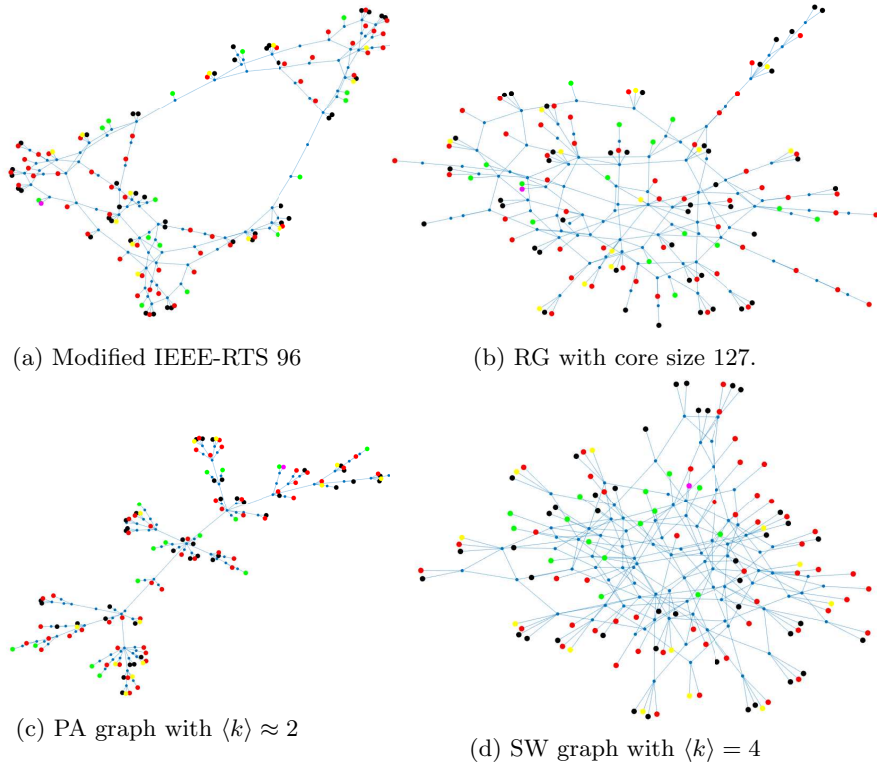(d) SW graph with $\langle k \rangle = 4$

Figure 1: Visualization of the test cases. Conventional generators are black nodes, PV-farms are yellow, wind farms are green, loads are red, and inner nodes are blue. All edges are the same color; the *real* edges connect two inner nodes (blue), while the *virtual* edges link an external node (non-blue node) to an inner one (blue).

i7-6600 U, 2.60 GHz, with 16 GB ram, running Windows 10 Pro. The longest MC simulation has run for 12h 10min and 20000 4-days iterations, while the shortest one for 1h 40 min and 2000 iterations. The running time of DC-load flow simulations for the siting of the optimal storage capacity varied between 1h 50 min and 5h, depending on the grid topology and siting policy. The MATLAB scripts developed for this work and the complete data set of results are available on request. A reduced data set is available in the electronic Appendix B.

7.1. Sizing of storage

The first goal of the simulations is to determine the optimal cost-effective size of storage that minimizes the expected OC, i.e., the total value of curtailed renewable energy and EENS. The storage considered in this work is megawatt-scale NaS system for energy-intensive application, whose all-inclusive cost of investment is 500 k€/ MWh [48]. The EAC, i.e. the costs per year of owning, operating, and maintaining a storage device over its entire expected life, of 8

different sizes are compared with the reduction in OC enabled by the use of storage, as shown in Figure 2.

The optimal storage has a power capacity equal to 20% of installed RES, i.e., $ch^{max} = 1200$ MW, and energy capacity $SoC^{max} = 7200$ MWh, given an energy to power ratio of 6 and $\eta_{ch} = \eta_{dis} = 87\%$ [48]. The convergence criterion is met after 5 037 iterations. Assuming the single busbar model of the modified IEEE-RTS 96 without any batteries as the baseline, the use of the optimal-sized storage reduces the EENS from 1304 ppm to 516 ppm (-60%) and the annual RES curtailment from 34.5 GWh to 31 MWh (-99.9%).
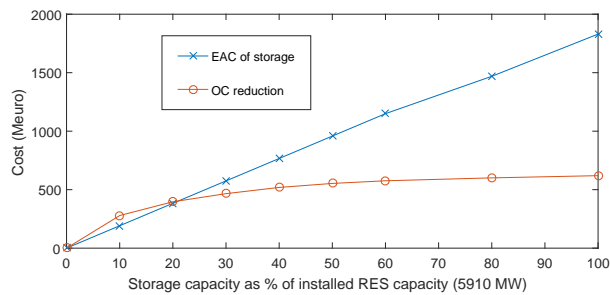

Figure 2: Cost-effectiveness of energy storage devices: equivalent annual costs of energy storage devices are compared with the reduction in OC enhanced by their use.

The storage exploitation in terms of power and energy is shown in Figure 3. As one can see, the power capacity is fully exploited in only 20 hours, considering both charging and discharging phases, during which roughly 12 GWh of renewable energy are saved, and 9 GWh of load shedding are avoided. The maximum recorded state of charge is about 85% of SoC^{max}.
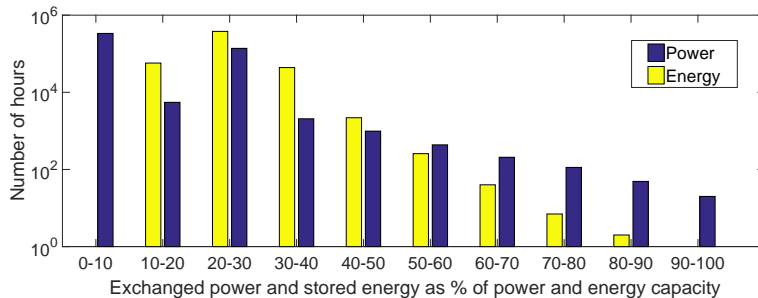

Figure 3: Storage exploitation: number of hours when stored energy and power exchanged with the grid are within the different percentages of energy and power capacities. $SoC^{min} = 0.1 SoC^{max}$. The hours are counted over 5 037 iterations. The storage is considered "fully exploited" when the exchanged power is $\geq 90\%$ of power capacity

7.2. The effects of different topologies

The next evaluation is investigating the topological effects. Eight grids with different topologies are used as test-cases to simulate how the power would flow, given the unit-commitment resulting from the operation phases. The influence of grid's structure on its performances is investigated, considering the case without storage as reference.

7.2.1. From single busbar model to constrained grids

The limited line capacities in Equation (26) and the constraint on flow-conservation at inner nodes in Equation (27) significantly affect the performances, as one can see in Table 3. The values of EENS and RES curtailment resulting from our simulations are higher than in actual systems, where the grids are designed and developed according to long-term load forecasting. The small-world grid with $\langle k \rangle = 4$ shows the lowest increases in $EENS_{year}$ and $Curt_{year}$, followed by the optimized IEEE-RTS 96 and the PA graph with $\langle k \rangle = 4$. As the network structure is neglected in the single busbar model, the only reason that can lead to load shedding is the shortage of power, which means that the available capacity is not enough to satisfy the request. On the contrary, when constrained graphs are considered, load shedding can be caused also by the limited transmission capacity and the non-existence of feasible solution. In the first case, only part of the load can be supplied due to the limited power that the lines can carry; in the second one, the GLPK solver cannot find a feasible solution, i.e., a solution to the optimization problem formulated in Equation (22) that satisfies all the constraints and bounds in Equation (23)-(31) [70]; hence, the hourly load is not fully met. In particular, this happens when using the modulation margin of conventional generators and curtailing RES output is still not sufficient to satisfy the node balance constraint and/or to keep the lines load below the LTR. The incidence of the three causes for load shedding is reported in Figure 4.

Table 3: GRID PERFORMANCES FROM SINGLE BUSBAR MODEL TO CONSTRAINED GRIDS

ID	Annual EENS	Annual Curtailment
SB	8.08E+04 MWh/y	3.46E+04 MWh/y
IEEE	+65%	+101%
RG	≥+350%	≥+350%
RG4	≥+350%	≥+350%
PA4	+178%	≥+350%
SW4	+58%	+85%
RG2	≥+350%	≥+350%
PA2	+317%	≥+350%
SW2	≥+350%	≥+350%

From single busbar model (SB) to constrained grids: increases in EENS and curtailment.

The lack of power is always the same if expressed in absolute value since the level of production of each unit is determined during the operation phases, but it has a greater impact on the grids for which the solver can always generate a feasible solution, i.e., SW4, IEEE, and PA4. Moreover, those cases never

experience an emergency state; in other words, it is always possible to run the DC-load flow keeping all lines within their LTR. Among those three grids, the PA4 has the highest EENS due to limited transmission capacity. Among the graphs with $\langle k \rangle \approx 2$, the PA2 shows the best results; for just 32 hours there is no solution to the power flow problem, which is less than 0.02% of the total number of time-steps, while RG2 and SW2 fail in 65% and 82% of cases. In all random graphs and in SW2, indeed, the non-existence of feasible solutions is responsible for more than 99% of total EENS. The increase in curtailed energy is tied to the higher energy not supplied since only renewable power can be limited to balance a lower demand.
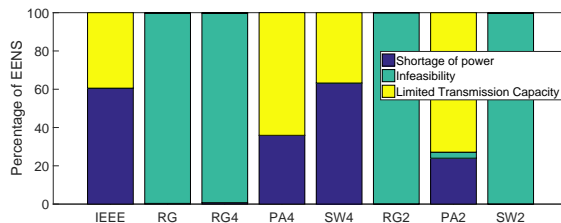

Figure 4: Load shedding causes: shortage of power, infeasibility, and limited transmission capacity. The incidence is expressed in % of the total expected energy not supplied.

7.2.2. Siting of storage devices

To identify the most stressed lines and the relevant nodes, the metrics introduced in Equations (1) and (2) are applied and averaged after running the DC-power flow of simulations without storage on each of the eight grids. Siting policies presented in Section 4.2 are employed to locate the batteries in every network, and the effects of their location on system reliability are compared, addressing our third objective.

First of all, some siting policies may turn out to be counter-productive when compared to the system's performances before storage's introduction. By comparing the variation of OC with EAC, in some solutions not even the optimal-sized storage is cost-effective. This is the case with all but "10 PTDF" siting policy in RG4, with the "10 loads" policy in RG, and with the "10 loads" and the centralized policies in RG2. Moreover, RG, RG4, RG2, and SW2 keep failing in a significant portion of hours, i.e., on average $> 24\%$, $> 15\%$, $> 65\%$, and $> 72\%$, respectively. Their output data are at least two orders of magnitude higher than of the other configurations, hence the comparability is limited. Consequently, the effects of different locations are investigated among four test-cases, i.e., IEEE, PA4, SW4, and PA2. The performances in terms of EENS and annual RES curtailment are shown in Figures 5a and 5b.

On average the major reductions in EENS and curtailed energy are achieved when decentralized batteries are located by means of PTDF matrices, with a mean decrease of -68.5% and -91.7% with respect to the scenarios without storage, respectively. This configuration is particularly successful with the PA4

(a) EENS with and without storage following four siting policies.

(b) Annual RES curtailment with and without storage following four siting policies.
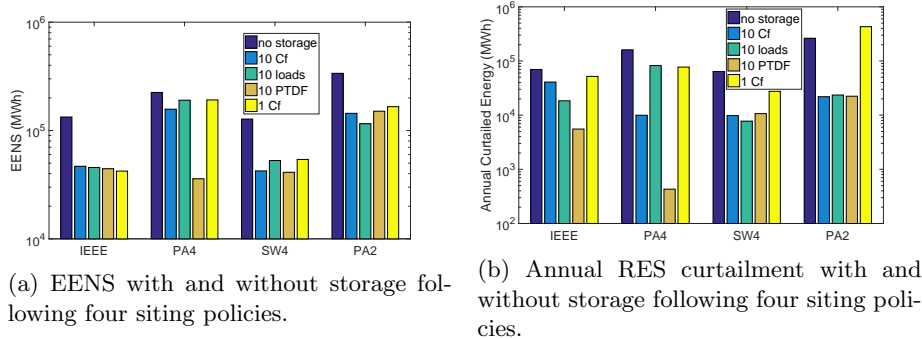
Figure 5: Effects of siting policies on four test-cases: performances in terms of EENS and annual RES curtailment

grid; this case not only shows the lowest annual values of EENS and curtailment, but it is also the only case always solved by keeping the power flow within the continuous rating of all lines. Among all grids, the IEEE-RTS 96 benefits the most from storage introduction, with an average improvement in satisfied load of +66.4%, followed by SW4 with +62.7%. The centralized solution works fine only for the IEEE grid, while it gives the worst results on the other networks. In particular, it significantly affects the PA2 performances, by almost doubling the time-steps with no feasible solution, from 32 to 60. On the contrary, all others siting policies improve them, resulting in zero failure with "10 C_f" and "10 loads" policies. These two configurations show comparable impact in terms of EENS and failures.

Regarding the curtailment of renewable energy, one can see in Figure 5b that the centralized policy is the worst in almost all scenarios. When considering PA2 grid, it scores even lower than the case without batteries (curtailment increases of +64%). As already noticed, on average the results of the PTDF-based policy are the best, with a significant margin for the IEEE and PA4 grids.

Lastly, the effects of the PTDF-based policy on line overloading are investigated. The most successful results are obtained in the PA4 grid. Without storage, this case did not experience any failures or emergencies, but ten lines were overloaded in several time-steps. After installing batteries according to the PTDF-based policy, all simulations are solved by keeping the lines within their CR, avoiding any risk of congestion. The PA2 and SW4 grid show good results in terms of lines in emergency state; in both cases, this policy assures the lowest number of records. A reduction in overloading states of three of the lines connecting main hubs in PA2 is also observed. Only with this configuration, in the IEEE-RTS 96, there are some hours with no feasible solution and multiple records of emergency states, though less than 20 ppm of all simulations.

8. Conclusions

In order to guarantee the continuity of supply and the security and reliability of the current and future electricity system, there is the need to manage the growing amount of renewable sources connected to high voltage networks. Real-time weather conditions and load demand can significantly diverge from expected ones, requiring to adjust the forecast operation to reduce the risk of unsupplied load and curtailment. The present work addresses this problem by investigating siting policies and economic consequences of adopting increasing amount of storage systems and different topological configurations for the grid.

The results show that NaS large-scale batteries can be cost-effective if their operation is oriented on reducing EENS and RES curtailment. For synthetic grids these values are worse than for actual grids, given the probabilistic element and that they are not designed for long-term load predictions. Nevertheless, if the graph-theoretical techniques we propose here are used in combination with long-term forecasting and actual grid needs, we expect to have a new generation of planning tools that will rely both on robust and efficient networks allowing for high penetration of renewables. Given the already declining trend in storage costs [18, 19], the operations of large-scale batteries could help to overcome the technical difficulties [5] and strong public opposition [6] that network renovation and expansion plans may encounter. The combination of the two techniques could be done as an extension of our previous work on modifying the topology of existing distribution networks [71].

From a topological point of view, when comparing grids with a weakly meshed structure and average degree 2, the existence of energy hubs significantly improves the capability of the network to work in secure state, and enables a more effective transmission within groups of sinks and sources connected to the same busbars. Among meshed networks, the small-world graph with $\langle k \rangle = 4$ shows the most successful results, actually even better than the optimized IEEE-RTS 96. Unlike the RG4, both SW4 and PA4 have small-world properties, confirming the efficiency in energy or, in general, information distribution among grids with small characteristic path length and large clustering coefficient [72, 58]. Additionally, it can be speculated that a more homogeneous distribution of edges among the nodes works better than having few nodes with a very high degree.

The siting analysis evidences that having one centralized storage is usually the worst solution, as demonstrated also in [23]. It may not be possible, indeed, to transfer all energy surplus from renewable farms scattered around the graphs to one single node. Among the other policies, the PTDF-based one is particularly successful and achieves on average the major reduction in EENS and RES curtailment. Looking at the modified IEEE-RTS 96, the slightly worse results in EENS (+5%) w.r.t. the centralized solution are more than compensated by the 90% increase in the use of renewable energy.

To conclude, although it is not possible to affirm the PTDF-policy is always the best for storage siting, it is definitely a valid approach when investigating these kinds of problems.

22

Appendix A. Monte Carlo method and probabilistic models

In the following, details about the applications of Monte Carlo method and the models for wind and solar production are briefly illustrated.

Appendix A.1. Conventional Generators' Availability and Power Demand

The MC technique has been largely used to study the behavior of power systems with a probabilistic approach (e.g., [61, 73, 74, 75]), taking into account more possible scenarios than with a deterministic method.

It is assumed that a generator can be described as a 2-state component, "available" or "unavailable," by means of two quantities called mean time to failure (MTTF) and mean time to repair (MTTR). The former indicates the length of time it is expected to last in operation before it fails. The latter indicates the average time required to be repaired. In this work, since a 24-hours horizon is considered, if a component fails during the day, it is considered to be out of order for the rest of the simulation. The values are taken from [64]. At each time step and for each component, a random number A between 0 and 1 is drawn from a uniform distribution [73] and the state of the component is determined as follows:

$$st_h = 1 \quad \text{if } st_{h-1} = 1 \text{ and } A > 1/MTTF \tag{A.1a}$$

$$st_h = 0 \quad \text{if } st_{h-1} = 0 \text{ or if } st_{h-1} = 1 \text{ and } A \leq 1/MTTF \tag{A.1b}$$

If $st_h = 1$ then the generator is available, otherwise it is out of order. As one can see, the state at time-step h depends on the state at the previous one h-1, hence it is a sequential version of the Monte Carlo technique.

To assess the real-time total consumer demand, the hourly forecasting error $e_{MC,h}$ is drawn by a normal distribution with mean value $\mu = 0$ and standard deviation $\sigma = 0.01$. The real-time demand is calculated considering the cumulative error of all previous time-steps, as $D_{real,h} = D_{ex,h} + \sum_{j=1}^{h} e_{MC,j} D_{ex,j}$.

Appendix A.2. Wind and Solar Production

The available wind production $P_{av,w,h}$ is determined by assuming a cubic-type dependency between wind speed and power output of a wind turbine, as follows:

$$P_{av,w,h} = \begin{cases} 0 & \text{if } w_{s,h} \leq v_{in} \text{ or } w_s \geq v_{off} & \text{(A.2a)} \\ P_r^{max}(w_{s,h}^3 - v_{in}^3)/(v_r^3 - v_{in}^3) & \text{if } v_{in} < w_s < v_r & \text{(A.2b)} \\ P_r^{max} & \text{if } v_r \leq w_{s,h} < v_{off} & \text{(A.2c)} \end{cases}$$

where $w_{s,h}$ is the wind speed at time-step h; v_r, v_n, and v_{off} are the rated, cut-in, and cut-off velocity of the wind turbine, respectively. In the forecasting phase, $w_{s,h}$ is expected to be equal to the mean seasonal speed at each time-step, while in real-time operation it is drawn by a Weibull probability distribution. Its shape and form parameters are chosen in order to give the best fit to the expected seasonal mean wind speed [76, 77].

The solar model takes into account the panels' location and seasonal condition. The solar radiation model is based on the simple sky model proposed in [78] and it is formulated as follows:

$$I_{s,h} = \begin{cases} 0 & \text{if } h \leq h_{sr} \text{ or } h \geq h_{ss} \quad \text{(A.3a)} \\ S_{max,s,h} sin\{\pi(h - h_{sr})/(h_{ss} - h_{sr})\} & \text{if } h_{sr} < h < h_{ss} \quad \text{(A.3b)} \end{cases}$$

where $I_{s,h}$ is the solar irradiance (MW/m^2) at time h, h_{sr} and h_{ss} are the sunrise and sunset time, respectively, and $S_{max,s,h}$ is the peak solar irradiance (MW/m^2). In this work, as the panels are located on terrestrial surface, $S_{max,s,h}$ is computed as the hourly maximum terrestrial irradiance $I_{Tmax,h}$ times the hourly clearness index $C_{s,h}$. $I_{Tmax,h}$ is a function of the peak value on terrestrial surface I_0, eccentricity factor E_0, and zenith angle $\theta_{z,h}$, as follows:

$$I_{Tmax,h} = I_0 E_0 cos\theta_{z,h} = (1000 \cdot 10^{-6})(1 + 0.033cos(2\pi d_n/365))cos\theta_{z,h} \quad \text{(A.4)}$$

where d_n is the number of the simulated days in the year. The zenith angle is calculated according to Algorithm 3 in [79] and it depends on the local time, position, pressure, and temperature. $C_{s,h}$ can be defined as the portion of sky not covered by clouds. Hourly values for each solar farms are drawn by a modified gamma distribution as proposed in [80, 79]. The maximum value of the index varies over the four representative days in order to take into account seasonal variability. Finally, assuming that the panels are always perpendicular to solar beams, the power output of an array of solar panels is expressed as $P_{s,h} = I_{s,h}S_s\eta_s$, where S_s and η_s are the surface (m^2) and efficiency of the array, respectively.

Appendix B. Supplementary data

Supplementary numerical data are reported and discussed in the online version of this paper.

Acknowledgment

References

[1] Eurostat (European Commission), Smarter, greener, more inclusive? Indicators to support the Europe 2020 strategy: 2016 edition, `http://ec.europa.eu/eurostat/en/web/products-statistical-books/-/KS-EZ-17-001` (2016).

[2] U.S. Department of Energy, 20% Wind energy by 2030, `http://www.nrel.gov/docs/fy08osti/41869.pdf` (2008).

[3] T. Broeer, J. Fuller, F. Tuffner, D. Chassin, N. Djilali, Modeling framework and validation of a smart grid and demand response system for wind power integration, Applied Energy 113 (2014) 199–207.

[4] A. L'Abbate, F. Careri, G. Migliavacca, Transmission expansion planning in presence of large RES penetration: The case of Italy, 2013 IEEE Grenoble Conference PowerTech.

[5] EPRI, Application of Storage Technology for Transmission System Support: Interim Report (2012).

[6] M. Eddy, Germany's clead-energy plan faces resistance to power lines, http://www.nytimes.com (2014).

[7] G. Giannuzzi, F. Bassi, M. Giuntoli, P. Pelacchi, D. Poli, Mechanical behaviour of multi-span overhead transmission lines under dynamic thermal stress of conductors due to power flow and weather conditions, International Review on Modelling and Simulations (IREMOS) 6 (4).

[8] M. Hedayati, J. Zhang, K. W. Hedman, Joint transmission expansion planning and energy storage placement in smart grid towards efficient integration of renewable energy, 2014 IEEE PES T&D Conference and Exposition (2014) 1–5.

[9] A. D. Del Rosso, S. W. Eckroad, Energy storage for relief of transmission congestion, IEEE Transactions on Smart Grid 5 (2) (2014) 1138–1146.

[10] N. Li, C. Uckun, E. M. Constantinescu, J. R. Birge, K. W. Hedman, A. Botterud, Flexible Operation of Batteries in Power System Scheduling with Renewable Energy, IEEE Transactions on Sustainable Energy 7 (2) (2016) 685–696.

[11] D. O. Akinyele, R. K. Rayudu, Review of energy storage technologies for sustainable power networks, Sustainable Energy Technologies and Assessments 8 (2014) 74–91.

[12] K. A. Zach, H. Auer, Bulk energy storage versus transmission grid investments: Bringing flexibility into future electricity systems with high penetration of variable RES-electricity BT - 9th International Conference on the European Energy Market, EEM 12, May 10, 2012 - May 1 (2012) 1–5.

[13] G. Graditi, M. G. Ippolito, E. Telaretti, G. Zizzo, Technical and economical assessment of distributed electrochemical storages for load shifting applications: An Italian case study, Renewable and Sustainable Energy Reviews 57 (2016) 515–523.

[14] M. Rosas-Casals, Power grids as complex networks. Topology and fragility, COMPENG 2010 (2010) 21–26.

[15] C. Brancucci Martínez-Anido, R. Bolado, L. De Vries, G. Fulli, M. Vandenbergh, M. Masera, European power grid reliability indicators, what do they really tell?, Electric Power Systems Research 90 (2012) 79–84.

[16] M. Giuntoli, P. Pelacchi, D. Poli, On the use of simplified reactive power flow equations for purposes of fast reliability assessment, in: Eurocon 2013, 2013, pp. 992–997.

[17] G. A. Pagani, From the grid to the smart grid, topologically, Ph.D. thesis, relation: http://www.rug.nl/ Rights: University of Groningen (2014).

[18] D. Manz, R. Walling, N. Miller, B. Larose, R. D'Aquila, B. Daryanian, The grid of the future: Ten trends that will shape the grid over the next decade, IEEE Power and Energy Magazine 12 (3) (2014) 26–36.

[19] Energy Storage Association, Energy Storage: Falling Costs, Major Gains, `http://energystorage.org/news/esa-news/energy-storage-falling-costs-major-gains` (2017).

[20] M. Korpaas, A. T. Holen, R. Hildrum, Operation and sizing of energy storage for wind power plants in a market system, International Journal of Electrical Power and Energy System 25 (2003) 599–606.

[21] A. Berrada, K. Loudiyi, Operation, sizing, and economic evaluation of storage for solar and wind power plants, Renewable and Sustainable Energy Reviews 59 (2016) 1117–1129.

[22] K. Dvijotham, M. Chertkov, S. Backhaus, Storage sizing and placement through operational and uncertainty-aware simulations, Proceedings of the Annual Hawaii International Conference on System Sciences (2014) 2408–2416.

[23] M. Ghofrani, A. Arabali, M. Etezadi-Amoli, M. Fadali, Energy storage application for performance enhancement of wind integration, IEEE Transactions on Power Systems 28 (4) (2013) 4803–4811.

[24] Z. Gao, P. Wang, L. Bertling, J. Wang, Sizing of energy storage for power systems with wind farms based on reliability cost and wroth analysis, IEEE Power and Energy Society General Meeting (2011) 1–7.

[25] P. Harsha, M. Dahleh, Optimal management and sizing of energy storage under dynamic pricing for the efficient integration of renewable energy, IEEE Transactions on Power Systems 30 (3) (2015) 1164–1181.

[26] Y. Zhang, S. Zhu, a. a. Chowdhury, Reliability modeling and control schemes of composite energy storage and wind generation system with adequate transmission upgrades, IEEE Transactions on Sustainable Energy 2 (4) (2011) 520–526.

[27] C. Root, H. Presume, D. Proudfoot, L. Willis, R. Masiello, Using battery energy storage to reduce renewable resource curtailment, 2017 IEEE Power and Energy Society Innovative Smart Grid Technologies Conference, ISGT 2017 (2017) 1–5doi:10.1109/ISGT.2017.8085955.

[28] L. Fiorini, G. A. Pagani, P. Pelacchi, D. Poli, M. Aiello, Sizing and siting of large-scale batteries in transmission grids to optimize the use of renewables, IEEE Journal on Emerging and Selected Topics in Circuits and Systems 7 (2) (2017) 285–294.

[29] H. Pandzic, Y. Wang, T. Qiu, Y. Dvorkin, D. S. Kirschen, Near-Optimal Method for Siting and Sizing of Distributed Storage in a Transmission Network, IEEE Transactions on Power Systems (2014) 1–13.

[30] S. Wogrin, D. F. Gayme, Optimizing Storage Siting, Sizing, and Technology Portfolios in Transmission-Constrained Networks, IEEE Transactions on Power Systems 30 (6) (2015) 3304–3313.

[31] M. Ghofrani, A. Arabali, S. Member, M. Etezadi-amoli, L. S. Member, M. S. Fadali, S. Member, A Framework for Optimal Placement of Energy Storage Units Within a Power System With High Wind Penetration 4 (2) (2013) 434–442.

[32] R. Konishi, M. Takahashi, Optimal allocation of photovoltaic systems and energy storages in power systems considering power shortage and surplus, 9th International: 2014 Electric Power Quality and Supply Reliability Conference, PQ 2014 - Proceedings (2014) 127–132.

[33] D. P. Chassin, C. Posse, Evaluating North American electric grid reliability using the Barabási-Albert network model, Physica A: Statistical Mechanics and its Applications 355 (2-4) (2005) 667–677.

[34] Å. J. Holmgren, Using graph models to analyze the vulnerability of electric power networks, Risk Analysis 26 (4) (2006) 955–969.

[35] E. Bompard, D. Wu, F. Xue, The concept of betweenness in the analysis of power grid vulnerability, COMPENG 2010 - Complexity in Engineering (2010) 52–54.

[36] P. Han, M. Ding, Analysis of Cascading Failures in Small-world Power Grid, International Journal of Energy Science IJES 1 (2) (2011) 99–104.

[37] G. A. Pagani, M. Aiello, The power grid as a complex network: a survey, Physica A: Statistical Mechanics and its Applications 392 (1) (2013) 2688–2700.

[38] G. A. Pagani, M. Aiello, Towards decentralization: A topological investigation of the medium and low voltage grids, IEEE Transactions on Smart Grid 2 (3) (2011) 538–547.

[39] G. A. Pagani, M. Aiello, A complex network approach for identifying vulnerabilities of the medium and low voltage grid, International Journal of Critical Infrastructures 7 11 (1) (2015) 36–61.

[40] F. James, A review of pseudorandom number generators, Computer Physics Communications 60 (3) (1990) 329–344.

[41] J. von Neumann, Various techniques used in connection with random digits, in: A. Householder, G. Forsythe, H. Germond (Eds.), Monte Carlo Method, National Bureau of Standards Applied Mathematics Series, 12, Washington, D.C.: U.S. Government Printing Office, 1951, pp. 36–38.

[42] R. L. Harrison, Introduction to monte carlo simulation, AIP Conference Proceedings 1204 (1) (2010) 17–21.

[43] M. Giuntoli, D. Poli, On the possible use of probabilistic techniques for purposes of short-term load dispatching, International Review of Electrical Engineering (IREE) 8 (4) (2013) 1243–1252.

[44] Terna, Dati statistici sull'energia elettrica in italia 2012, `http://www.terna.it/archiviodocumenti.aspx`.

[45] A. O'Sullivan, S. Sheffrin, Economics: Principles in Action, Prentice Hall Science/Social Studies, Pearson/Prentice Hall, 2007.

[46] G. Fitzgerald, J. Mandel, J. Morris, H. Touati, The Economics of Battery Energy Storage: how multi-use, customer-sted batteries deliver the most services and value to customers and the grid (October) (2015) 41.

[47] A. Castillo, D. F. Gayme, Grid-scale energy storage applications in renewable energy integration: A survey, Energy Conversion and Management 87 (2014) 885–894.

[48] EPRI, Electric Energy Storage Technology Options - A Primer on Applications, Costs & Benefits (2010).

[49] X. Luo, J. Wang, M. Dooner, J. Clarke, Overview of current development in electrical energy storage technologies and the application potential in power system operation, Applied Energy 137 (2015) 511–536.

[50] M. Ceraolo, G. Lutzemberger, D. Poli, Aging evaluation of high power lithium cells subjected to micro-cycles, Journal of Energy Storage 6 (2016) 116–124.

[51] M. Newman, Networks: An Introduction, Oxford University Press, Inc., New York, NY, USA, 2010.

[52] P. Wong, P. Albrecht, R. Allan, et al., The IEEE Reliability Test System-1996. A report prepared by the Reliability Test System Task Force of the Application of Probability Methods Subcommittee, Power Systems, IEEE Transactions on 14 (3) (1999) 1010–1020.

[53] S. Arianos, E. Bompard, a. Carbone, F. Xue, Power grid vulnerability: a complex network approach., Chaos: An Interdisciplinary Journal of Nonlinear Science 19 (2009) 13119.

[54] C.-S. Song, C.-H. Park, M.-H. Yoon, G.-S. Jang, Implementation of PTDFs and LODFs for Power System Security, Journal of International Council on Electrical Engineering 1 (1) (2011) 49–53.

[55] L. C. Freeman, S. P. Borgatti, D. R. White, Centrality in valued graphs: A measure of betweenness based on network flow, Social Networks 13 (2) (1991) 141–154.

[56] X. Cheng, T. J. Overbye, PTDF-based power system equivalents, IEEE Transactions on Power Systems 20 (4) (2005) 1868–1876. doi:10.1109/TPWRS.2005.857013.

[57] D. J. Watts, S. H. Strogatz, Collective dynamics of 'small-world' networks, Nature 393 (6684) (1998) 440–442.

[58] M. D. Humphries, K. Gurney, Network 'small-world-ness': A quantitative method for determining canonical network equivalence, PLoS ONE 3 (4).

[59] Wind EUROPE, Windeurope views on curtailment of wind power and its links to priority dispatch.
URL https://windeurope.org/wp-content/uploads/files/policy/position-papers/WindEurope-Priority-Dispatch-and-Curtailment.pdf

[60] M. de Nooij, C. Koopmans, C. Bijvoet, The value of supply security, Energy Economics 29 (2) (2007) 277 – 295.

[61] R. Billinton, W. Li, Reliability Assessment of Electric Power Systems Using Monte Carlo Methods, Springer US, 1994.

[62] M. A. d. R. Armando M. Leite da Silva, Luiz Antônio F. Manso, Silvan A. Flávio, L. C. Resende, Composite Reliability Assessment of Power Systems with Large Penetration of Renewable Sources Armando (2013) 107–1028.

[63] C. B. Smith, K. E. Parmenter, Energy, management, principles: Applications, benefits, savings, Elsevier, 2013.

[64] H. Pandzic, Y. Dvorkin, T. Qiu, Y. Wang, D. Kirschen, Unit Commitment under Uncertainty - GAMS Models, Library of the Renewable Energy Analysis Lab (REAL), http://www.ee.washington.edu/research/real/library.html.

[65] P. Erdös, A. Rényi, On random graphs, Publicationes Mathematicae 6 (1959) 290–297.

[66] A.-L. Barabási, R. Albert, Emergence of Scaling in Random Networks, Science 286 (October) (1999) 509–512.

[67] N. Giorgetti, GLPKMEX A Matlab MEX interface for the GLPK library, `http://glpkmex.sourceforge.net/`.

[68] MIT Strategic Engineering, MATLAB tools for network analysis, `http://strategic.mit.edu`.

[69] Peregrine HPC cluster, `https://redmine.hpc.rug.nl/redmine/projects/peregrine`.

[70] D. Rader, Deterministic Operations Research: Models and Methods in Linear Optimization, John Wiley & Sons, 2010.

[71] G. Pagani, M. Aiello, From the grid to the smart grid, topologically, Physica A: Statistical Mechanics and its Applications 449 (5) (2016) 160–175.

[72] Ke Sun, Complex Networks Theory: A New Method of Research in Power Grid, 2005 IEEE/PES Transmission & Distribution Conference & Exposition: Asia and Pacific (2005) 1–6.

[73] P. Pelacchi, D. Poli, The influence of wind generation on power system reliability and the possible use of hydrogen storages, Electric Power Systems Research (2009) 1–13.

[74] S. Conti, S. Raiti, Probabilistic load flow using Monte Carlo techniques for distribution networks with photovoltaic generators, Solar Energy 81 (12) (2007) 1473–1481.

[75] M. A. Ortega-Vazquez, D. S. Kirschen, Estimating the spinning reserve requirements in systems with significant wind power generation penetration, IEEE Transactions on Power Systems 24 (1) (2009) 114–124.

[76] U. Ayr, Wind data analysis and wind energy potential in Italy, International Scientific Journal of Environmental Science 3 (3).
URL `http://environment.scientific-journal.com/articles/3/27.pdf`

[77] G. Carpinelli, P. Caramia, P. Varilone, Multi-linear Monte Carlo simulation method for probabilistic load flow of distribution systems with wind and photovoltaic generation systems, Renewable Energy 76 (2015) 283–295.

[78] T. Sung, S. Y. Yoon, K. C. Kim, A mathematical model of hourly solar radiation in varying weather conditions for a dynamic simulation of the solar organic rankine cycle, Energies 8 (7) (2015) 7058–7069.

[79] R. Grena, Five new algorithms for the computation of sun position from 2010 to 2110, Solar Energy 86 (5) (2012) 1323–1337.

[80] K. G. T. Hollands, R. G. Huget, A probability density function for the clearness index, with applications, Solar Energy 30 (1983) 195–209.